JOURNAL OF PROPULSION AND POWER
Vol. 12, No. 3, May–June 1996

Laboratory-Scale Hybrid Rocket Motor Uncertainty Analysis

R. A. Frederick Jr.* and B. E. Greiner†
University of Alabama in Huntsville, Huntsville, Alabama 35899

Laboratory-scale hybrid rocket motors often provide the means to evaluate the burning rates of new fuel formulations. While the issue of scaling to larger sizes can be significant, the uncertainty level of the laboratory-scale results also needs evaluation. This work quantitatively evaluates the uncertainty of key experimental results for a particular hybrid rocket motor. The scope includes calculation of the uncertainties in the fuel regression rate, oxidizer flux, motor characteristic velocity, and the oxidizer-to-fuel mass ratio for a laboratory-scale motor. The motor burned gaseous oxygen and hydroxyl-terminated polybutadiene at conditions characteristic of a preburner. The accepted uncertainty methodology of Coleman and Steele established the approach for the study. The results show that the typical uncertainty values are ±8.7% in the determination of the fuel regression rate, ±10.8% in the oxidizer flux, ±10.5% for motor characteristic velocity, and ±9.2% for the oxidizer-to-fuel ratio. Measurement uncertainties in the diameters of the initial fuel grain, initial port, and nozzle throat contributed significantly to these conclusions. Conceptual biases in determining the burn duration, the average chamber pressure, and the average burning rate have a significant influence. This evaluation revealed the important measurement limitations and potential improvements for the particular test conditions and data reduction equations used. However, the methodology presented is in generally applicable to hybrid rocket testing.

Nomenclature

B_α = bias (fixed) uncertainty in parameter α
C_d = metering venturi discharge coefficient
C^* = characteristic velocity, ft/s
D_i = initial fuel grain port diameter, in.
D_{th} = throat diameter of motor nozzle, in.
D_{vent} = throat diameter of metering venturi, in.
G_{ox} = gaseous oxygen mass flux, lbm/in.$^2 \cdot$ s
L = fuel grain total length, in.
l = aft mixing section length, in.
m_f = final mass of fuel grain, lbm
m_i = initial mass of fuel grain, lbm
O/F = mass ratio of oxidizer to fuel
P_c = average chamber pressure, psia
P_{up} = average pressure upstream metering venturi, psia
P_α = precision (random) uncertainty in α
R = gas constant for oxygen, 48.29 (ft lbf/(lbm R)
$\dot{r}$ = average fuel regression rate, in./s
T_{up} = average temperature upstream of venturi, R
t_f = shutdown time, s
t_i = ignition time, s
U_α = total uncertainty in component α
x_i = test input parameter
Δm = change in fuel grain mass, lbm
Δr = change in fuel grain port radius, in.
Δt = change in time, s
Γ = $\sqrt{\gamma[2/(\gamma+1)]^{(\gamma+1)/(\gamma-1)}}$
γ = specific heat ratio for oxygen
μ = mean value
π = pi, 3.141592654 . . .
ρ_f = density of solid fuel component, lbm/in.^{3}
σ = standard deviation

Presented as Paper 95-3085 at the AIAA/SAE/ASME/ASEE 31st Joint Propulsion Conference and Exhibit, San Diego, CA, July 10–12, 1995; received July 27, 1995; revision received Dec. 18, 1995; accepted for publication Jan. 6, 1996.

*Assistant Professor, Propulsion Research Center, Department of Mechanical and Aerospace Engineering, RI E-29. Senior Member AIAA.

†Graduate Research Assistant, Propulsion Research Center, Department of Mechanical and Aerospace Engineering, RI E-17. Student Member AIAA.

Introduction

CLASSICAL hybrid rocket motors use an inert solid fuel grain and a gaseous or liquid oxidizer. In the initial phases of fuel development programs, experimenters choose laboratory-scale[1] test motors to screen the burning rates of candidate fuel/oxidizer combinations. From these laboratory-scale tests, some information is also determined about the basic operational phenomena and combustion physics. Some correlation between laboratory-scale and full-scale burning rate results has been offered.[2] However, until recently, little more than an afterthought has been given to the experimental uncertainty of the laboratory-scale data on which the empirical correlations are based. With rare exception,[3] this is also the case with full-scale design and testing of hybrid rocket motors.

A test program on the mechanisms of hybrid rocket instability led to the uncertainty analysis of the laboratory-scale hybrid motor (LHM) used in the investigation.[4,5] The motor burned gaseous oxygen and a hydroxyl-terminated polybutadiene (HTPB) fuel. It operated at oxidizer-to-fuel ratios of 3.0, characteristic of a preburner motor. The data reduction equations for burning rate use finite difference values determined at the beginning and end of the test. This study included estimating the bias and precision levels for each measured parameter. The resulting uncertainty levels of the oxidizer flux, fuel regression rate, characteristic velocity, and oxidizer-to-fuel ratio were then determined by analyzing data reduction equations.

Uncertainty in an experimental result is based on estimates of the input parameter uncertainties. These include determining bias and precision limits. Also, there are conceptual biases that represent errors in the results induced by assumptions in the method. An example would be assuming linear behavior between two times when the behavior is, in fact, nonlinear. Thus, the total uncertainty is both a function of the particular instrumentation and the data reduction method for the experiment that is evaluated.

This article details the experimental uncertainty analysis that was performed on the LHM by describing 1) the experimental motor hardware and data acquisition system, 2) the develop-

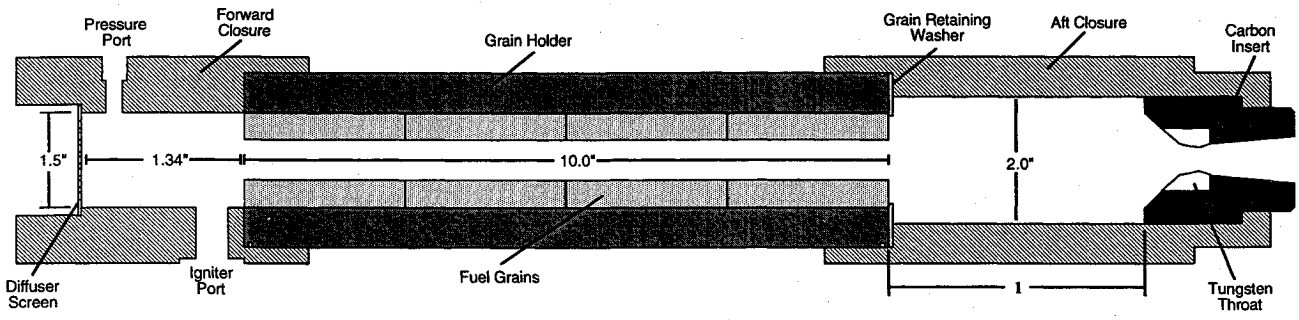

Fig. 1 Sketch of LHM layout.

ment of the data reduction and uncertainty equations, and 3) the analysis of the results from these equations.

Experimental Setup

The LHM hardware consisted of a forward closure, a grain holder, and an aft closure, as shown in Fig. 1. A gaseous oxygen feed system was connected to the motor at the forward closure. The grain holder surrounds cartridge-loaded fuel grains that are held in place by a retaining washer at each end of the grain holder. The aft mixing section consisted of an aft closure and a carbon insert surrounding a tungsten nozzle. The LHM offered flexibility in selecting various lengths of l in Fig. 1, different nozzle diameters, and different grain lengths.

During operation of the LHM, gaseous oxygen was injected in the forward end of the motor and diffused by the forward closure diffuser screen. The gaseous oxygen flow rate was controlled by a dome-loaded pressure regulator upstream of a metering venturi. After a 10-s oxygen preflow, a current applied to an NSI squib in the forward closure ignited the fuel. The squib had 114 mg of pyrotechnic material and a burning time of 16 ms. After a burning time of approximately 2 s, the oxygen flow was terminated and a nitrogen purge-flow was initiated to ensure complete extinguishment of the fuel surface. Short burning times were used because of the thermal limits of the uncooled tungsten nozzles used for these experiments.

The primary type of fuel used in the test firings was HTPB. Standard operating procedure called for four grains, which were cartridge loaded in the fuel grain holder. Each grain was nominally 2.5 in. long, had a 0.820-in.-diam port, and had a 1.375-in. o.d. The HTPB(R-45)/N-100 fuel grains ($C_{6.939}H_{9.855}N_{0.178}O_{0.264}$) were mixed and cast under a vacuum in phenolic sleeves. The castings were then cured for 24 h at 140°F.

The instrumentation used for the LHM experiments supplied data on the motor pressures, temperatures, and oxygen flow rate. Forward and aft pressure transducers were used to measure the pressures inside the motor. The pressure and temperature of the incoming oxygen were measured upstream of a choked metering venturi to determine the oxidizer mass flow rate. The various measurements were recorded on a digital system (0–40 Hz) and on an analog FM tape system.

The motor chamber pressure data were obtained from the test analog data recordings. The analog data were passed through a 5-kHz antialiasing filter and then digitized at 10 kHz. These high-frequency data were calibrated using the low-frequency data since the calibration techniques used on the analog system were found to be unacceptable. Instead, the calibration technique employed two pairs of corresponding points from the high-frequency data (voltage time) and the low-frequency data (pressure time). This produced a linear calibration curve. The technique of calibrating using the low-frequency data introduced a ±10-psia bias uncertainty into the high-frequency data because of the scatter of the high-frequency data at the calibration points. These data were used for qualitative visual analysis as well as for digital analysis of the frequency content through the use of fast Fourier transform (FFT) techniques. The motor operating times were also determined from the high-frequency digital data. A precision balance was used to weigh each fuel grain pre- and posttest to determine the average regression rate.

Analysis of Labscale Uncertainty

Using methods established by Coleman and Steele,[6] an experimental uncertainty analysis was performed to determine the uncertainty in the experimental results and to determine the important data reduction parameters in LHM testing. The basic uncertainty technique consists of determining the sensitivity of the data reduction equations to each input parameter, multiplying by the parameter bias limit, calculating the precision limit from the standard deviation of the test data, and combining these values in a rss form to determine overall uncertainty. To carry out this analysis, the equation for the experimental value of interest must be written explicitly in terms of measurable or input parameters. The development and results of these calculations are shown in the following sections for all of the data reduction equations.

Reduction of Data

Test data were reduced to determine the actual oxygen mass flux, average fuel burning rate, characteristic velocity, and oxidizer-to-fuel ratio during each test. The following equations express each of these results in terms of data measured from each test. The data reduction equations are all based on finite difference approximations of the results from data measured over the duration of the test. The full development of the data-reduction equations used in this article is detailed in Ref. 4.

The oxidizer mass flux was determined from measurements of the average temperature and pressure upstream of the oxygen venturi, and the initial and final propellant mass:

$$G_{ox} = \frac{2C_d P_{up} D_{vent}^2 \Gamma}{\{[4(m_i - m_f)/\pi\rho_f L] + 2D_i^2\}\sqrt{RT_{up}}} \tag{1}$$

For the calculation of regression rate, the mass consumption was assumed to occur evenly only over the fuel grain bore surface during the firing. This assumption is reasonable because of the short burning times used in this investigation, but under the additional assumption that the ignition and shutdown transients were small compared to the burning times. This leads to the following equation for the average regression rate (finite difference method):

$$\dot{r} \approx \frac{\Delta r}{\Delta t} = \frac{\sqrt{[4(m_i - m_f)/\pi\rho_f L] + D_i^2} - D_i}{2(t_f - t_i)} \tag{2}$$

In studies of instabilities it is sometimes useful to examine combustion efficiency. This may be accomplished by dividing the actual motor characteristic velocity by the theoretical at the same actual O/F ratio. The overall O/F ratio in this investigation was found by taking the ratio of the oxidizer and fuel mass flow rates:

$$O/F = \frac{C_d P_{up} \pi D_{vent}^2 \Gamma / 4\sqrt{RT_{up}}}{(m_i - m_f)/(t_f - t_i)} \tag{3}$$

This leads to the data reduction equation for the calculation of actual characteristic velocity:

$$C^* = \frac{P_c(\pi/4)D_{th}^2}{(C_d P_{up}\pi D_{vent}^2\Gamma/4\sqrt{RT_{up}}) + [(m_i - m_f)/(t_f - t_i)]} \quad (4)$$

Generalized Uncertainty Analysis

The first phase of an uncertainty analysis is the development of expressions for the values of interest from the data reduction equations. For brevity, the following expressions for the experimental uncertainty of the LHM are detailed using the gaseous oxidizer flux [Eq. (1)] as an example. These uncertainty expressions can then be examined to determine the critical or dominant test parameters.

First, the basic equation for the uncertainty must be considered. For G_{ox}, the generalized uncertainty equation is written:

$$U_{G_{ox}} = \sqrt{B_{G_{ox}}^2 + P_{G_{ox}}^2} \quad (5)$$

where $B_{G_{ox}}$ represents the total bias or fixed uncertainty limit in G_{ox}, which includes the contributions to the overall uncertainty that are constant from test to test. $P_{G_{ox}}$ represents the precision or random uncertainty limit for G_{ox}, which is the contribution from the statistically random scatter in the data.

The concepts of $B_{G_{ox}}$ and $P_{G_{ox}}$ are demonstrated by an illustration. Figure 2 shows a Gaussian distribution of flux readings centered about a point offset from the true value of G_{ox} by an amount equal to the bias limit $B_{G_{ox}}$. The methodology used to determine the bias limit is discussed in the following paragraphs. The precision limit $P_{G_{ox}}$ is found by determining the standard deviation, or σ, of the data about the mean value μ at a single set point and then doubling it to obtain the 95% confidence or 2σ interval. This is the limit within which one can be confident that 95% of the readings will lie. For this investigation, the scatter in results from test to test was considered to be because of slight uncontrollable differences in test parameters such as the venturi upstream pressure and temperature. This scatter is incorporated into the precision limit estimate by calculating the value of σ for the test results.

To calculate the bias limit for G_{ox}, one must determine how the uncertainty of each input parameter propagates into the bias limit. As stated earlier, this is accomplished by first writing the data reduction equation for the result of interest explicitly in terms of measurable input parameters.

In Eq. (1), it is seen that the input parameters are C_d, P_{up}, D_{vent}, γ, m_i, m_f, ρ_f, L, D_i, and T_{up}. From Ref. 3, the expression for the propagation of the bias uncertainties of the data reduction equation input parameters x_i into G_{ox} is written:

$$B_{G_{ox}}^2 = \sum_i \left(\frac{\partial G_{ox}}{\partial x_i} B_{x_i}\right)^2 \quad (6)$$

where the partial derivative term is simply the sensitivity of G_{ox} to parameter x_i and is determined for each parameter from the basic data reduction equation for G_{ox}. Equation (6) has the additional assumption that correlated biases between parameters, if they exist, are negligible. Expanding Eq. (6) using Eq. (1):

$$B_{G_{ox}}^2 = \left(\frac{\partial G_{ox}}{\partial C_d} B_{C_d}\right)^2 + \left(\frac{\partial G_{ox}}{\partial P_{up}} B_{P_{up}}\right)^2 + \left(\frac{\partial G_{ox}}{\partial D_{vent}} B_{D_{vent}}\right)^2 + \left(\frac{\partial G_{ox}}{\partial \gamma} B_\gamma\right)^2 + \sum_{j=1}^{4}\left(\frac{\partial G_{ox}}{\partial m_i} B_{m_i}\right)_j^2 + \sum_{k=1}^{4}\left(\frac{\partial G_{ox}}{\partial m_f} B_{m_f}\right)_k^2 + \left(\frac{\partial G_{ox}}{\partial \rho_f} B_{\rho_f}\right)^2 + \left(\frac{\partial G_{ox}}{\partial L} B_L\right)^2 + \left(\frac{\partial G_{ox}}{\partial D_i} B_{D_i}\right)^2 + \left(\frac{\partial G_{ox}}{\partial T_{up}} B_{T_{up}}\right)^2 \quad (7)$$

Note that for the fuel grain mass terms, a summation is included to account for the bias limits in the individual fuel grains.

Zero-Order Uncertainty Analysis

An indication of the relative importance of each input parameter can be determined by conducting a zero-order uncertainty analysis. In this analysis the precision uncertainties are neglected and the bias uncertainties in the individual parameters are assumed to be 1% of the nominal parameter value. The partial derivatives were calculated to determine the parameter sensitivities. Because of the relative complexity of the data reduction equations, a finite difference technique was used to approximate these derivatives. These calculations were carried out for each test and each data reduction equation using a spreadsheet utility. Table 1 shows the results of these calculations for the individual G_{ox} parameters on a nominal HTPB test.

Combining the terms in the last column of Table 1, according to Eq. (7), the overall bias for G_{ox} using the zero-order analysis is ± 0.0093 lbm/in.^{2}·s or $\pm 3.0\%$ of nominal. Comparing this to the results in the last column of Table 1, one can see that the uncertainty in G_{ox} is strongly dominated by the propagation of uncertainties in D_{vent} and D_i. Uncertainties in C_d, P_{up}, and γ are minor contributors, while the remaining input parameters (m_i, m_f, ρ_f, L, and T_{up}) have only a weak influence. This analysis indicates that by minimizing uncertainties in D_{vent} and D_i, and to some extent C_d, P_{up}, and γ, the uncertainty in G_{ox} is minimized. The results also show that the other parameters can be neglected so long as the magnitudes of their uncertainties are equal to or less than those of the dominant parameters on a percent of nominal basis. Table 2 shows the results of the zero-order analysis on all of the data reduction equations. The double checks represent the dominant input parameters, single checks are the minor contributors, blanks show a weak influence, and the dash indicates that the particular data reduction equation is independent of that input parameter.

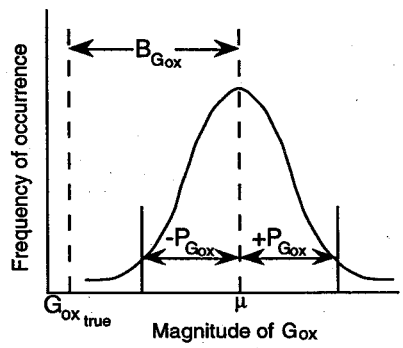

Fig. 2 Illustration of bias and precision uncertainty limits.

Table 1 Zero-order uncertainty analysis results or G_{ox} using 1% nominal uncertainties

x_i	$\frac{\partial G_{ox}}{\partial x_i}$	1% of nominal	$\frac{\partial G_{ox}}{\partial x_i} B_{x_i}$
D_{vent}	6.151	0.001	0.00615
D_i	−0.613	0.0082	−0.00502
C_d	0.327	0.02	0.0031
P_{up}	0.0002	11	0.0024
T_{up}	−0.003	5.25	−0.0015
γ	0.0763	0.0139	0.0011
m_i	−0.0016	0.50	−0.0008
m_f	0.0016	0.41	0.0006
ρ_f	1.673	0.0003	0.0006
L	0.0056	0.1	0.0006

Table 2 Results of zero-order analysis on data reduction equations

	Input parameters														
Result	C_d	P_{up}	T_{up}	D_{vent}	γ	m_i	m_f	ρ_f	L	D_i	t_i	t_f	D_{th}	P_c	% bias
G_{ox} (1)	√	√	√	√√	√					√√	—	—	—	—	±3.0
$\dot{r}$ (2)	—	—	—	—	—	√	√	√	√	√	√	√	—	—	±3.9
O/F (3)	√	√		√√		√	√	—	—	—	√	√	—	—	±4.6
C^* (4)		√		√√				—	—	—			√√	√	±3.0

Table 3 Representative precision limits in experimental results

Experimental result	P_α	% of nominal
G_{ox} (1)	±0.00489	±1.6
$\dot{r}$ (2)	±0.001158	±2.9
O/F (3)	±0.296	±5.8
C^* (4)	±317.2	±6.8

Table 4 Estimate of input parameter bias limits for LHM detailed analysis of G_{ox}

Input parameter	B_α	% of actual
C_d	±0.02	±2.1
D_{vent}	±0.001	±1.0
P_{up}	±5	±0.5
T_{up}	±10	±1.9
γ	±0.05	±3.6
m	±0.0005	±0.0001
ρ_f	±0.004	±11.9
L	±0.05	±0.5
D_i	±0.05	±6.1
D_{th}	±0.005	±1.6
P_c	±10	±2.1
t_i	±0.035	±1.8
t_f	±0.115	±5.8

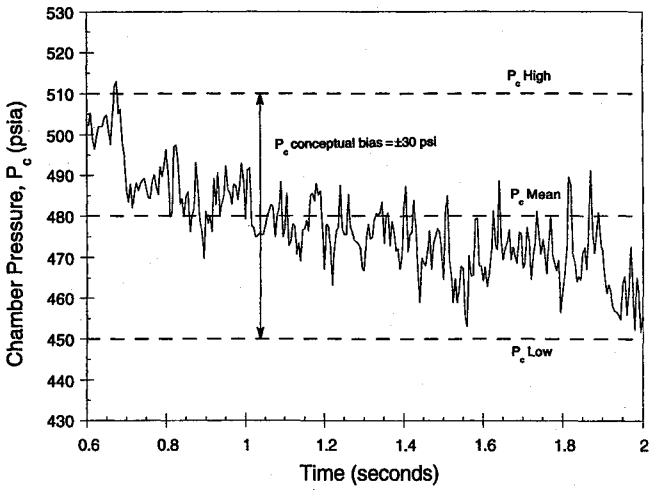

Fig. 3 Illustration of chamber pressure.

Detailed LHM Uncertainty Analysis

The next step in the examination of the LHM uncertainty was to perform the detailed analysis. This is a refining-type analysis that is performed once test data are taken, and that permits the calculation of the precision index, or 2σ, and a better estimate of the system biases. Table 3 shows representative values of the precision limits for the different data reduction results as well as the precision uncertainty as a percent of the nominal resultant value.

Table 4 shows the estimates of the input parameter bias limits in absolute magnitude as well as a percentage of actual value for a representative HTPB test. The estimates of the individual biases were made at a 95% confidence level. The biases for D_{vent} and C_d were based on the venturi manufacturer's specifications. For P_{up} and T_{up}, biases were based on the calibration specifications and on fluctuations of conditions during tests. The bias in γ was based on scatter in published values for oxygen. The bias for the mass measurements was based on the accuracy of the digital analytical scale used to weigh the grains. The fuel grain length bias was taken from the accuracy of the calipers used to measure the grains. For the fuel density, the bias was estimated based on scatter in accepted density values. The bias in the initial port diameter was estimated based on the casting mandrel tolerances. The bias in D_{th} was based on manufacturing drawing tolerances.

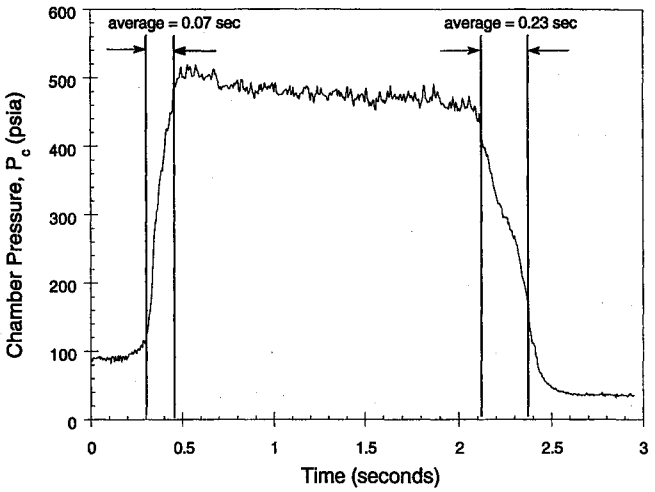

Fig. 4 Illustration of burning duration conceptual bias.

As stated earlier, a bias of ±10 psi was introduced in the measurement of chamber pressure because of the methodology used for calibration of the test data. However, an additional, more dominant bias because of a conceptual uncertainty in the definition of chamber pressure was present in the testing as well. This is illustrated in Fig. 3. Uncertainty in the chamber pressure measurement (which was entered in the data reduction equations as the mean pressure), was

$$\sum_i \left(\frac{\partial G_{ox}}{\partial x_i} B_{x_i}\right)^2$$

primarily because of oscillations and drops or rises in pressure during the burn duration. On average, this conceptual bias was ±30 psi. Using the rss method of combining the conceptual and calibration biases gave a total bias in chamber pressure of ±31.6 psi.

The primary contribution to the bias in the ignition and shutdown times was a conceptual uncertainty in the definition of burning time. This concept is illustrated in Fig. 4, which shows the pressure–time plot for a typical HTPB test conducted using an aft mixing section with l = 4.0 in. (see Fig. 1). Detailed in Fig. 4 are the two regions within which it may safely be assumed the ignition and shutdown points lie. These two regions were from test to test, and on average, 0.07 and 0.23 s

Table 5 Detailed LHM uncertainty analysis results for a typical test

	Input parameters														
Result	C_d	P_{up}	T_{up}	D_{vent}	γ	m_i	m_f	ρ_f	L	D_i	t_i	t_f	D_{th}	P_c	% bias	% uncertainty
G_{ox} (1)	√			√						√√	—	—	—	—	±10.7	±10.8
$\dot{r}$ (2)	—	—	—	—	—					√√	√	√√	—	—	±8.2	±8.7
O/F (3)	√			√				—	—	—	√	√√	—	—	±7.1	±9.2
C^* (4)			√	√	√			—	—	—		√	√√	√√	±8.2	±10.5

long, consecutively. According to convention, the bias limit for each region is therefore one-half the span, or ±0.035 and ±0.115 s, as shown in Table 4.

Taking the values from Table 4 and substituting them into Eq. (7) gives a bias limit for a typical G_{ox} test of ±0.032 lbm/in.^{2}·s (for this particular test, G_{ox} = 0.319 lbm/in.^{2}·s), or approximately ±10.7%. Next, substituting this bias value and precision limit for G_{ox} from Table 3 into Eq. (5) gives an overall uncertainty limit for G_{ox} of ±0.0324 lbm/in.^{2}·s, or ±10.8%. The uncertainty values vary slightly from test to test because of the dependence of the sensitivity parameters to the actual test conditions.

Table 5 shows the results of similar calculations carried out in Eqs. (2–4) for the same test. Shown in the last two columns are the bias and total uncertainty limits in terms of percent of the data reduction result. By examining plots of the results generated from the reduction of the LHM data, with error bars included to represent the uncertainty in the results, and by examining and comparing Tables 1–5, one can note several items that are indicative of the behavior of hybrid testing.

Discussion

The results are now discussed along with suggestions for lowering the uncertainty levels.

Fuel Burning Rate

Figure 5 shows the typical hybrid plot of $\dot{r}$ vs G_{ox}. The points presented without uncertainty bars and the curve fit are taken from Sutton.[7] Our results are presented with uncertainty bars. The Sutton results are from a similar LHM. One of the indications of Fig. 5 is that the majority of the data generated by our LHM, within the uncertainty of the results, falls within the scatter of the Sutton data. However, there is actually a family of curve fits that could fall within the uncertainty limits of the data. Further, once a curve fit is generated, the level of uncertainty associated with the data is lost without knowledge of the original data. This demonstrates the limitations of using a burn rate equation based on laboratory-scale data.

By comparing the precision and bias limits (Tables 3 and 5), one can see that the overall uncertainties of the regression rate and flux measurements are dominated by the bias limits, indicating good repeatability. In a closer examination of Table 5, the primary contributors to the uncertainty in the data points in Fig. 5 are the measurement of the initial port diameter and the conceptual bias of the shutdown transient time. This points toward two methods to reduce the uncertainty in this type of plot. The first is to reduce the uncertainty in the measurement of the port diameter by either increasing the size of the fuel grain or increasing the measurement accuracy. The second is to reduce the uncertainty in the burning times. This can only be accomplished by increasing the burning duration since the bias itself is conceptual rather than because of any measurement inaccuracy. Increasing the duration reduces the sensitivity of the regression rate equation to the conceptual bias, even though the bias itself remains the same.

While increasing the test time can decrease its uncertainty, it also increases a conceptual bias in the determination of the burning rate. Assuming the burning rate equation $\dot{r} = aG_{ox}^n$, the burning rate determined by the change in mass over the

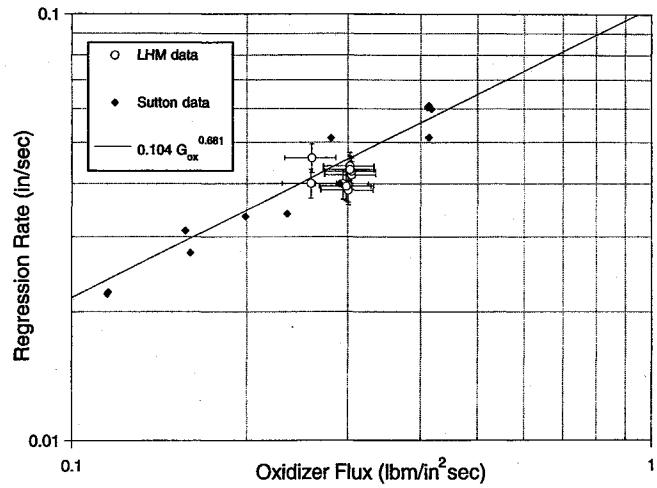

Fig. 5 Plot of regression rate vs oxidizer flux with uncertainty bars.

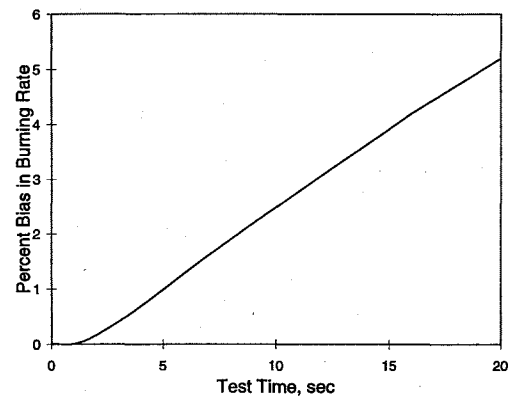

Fig. 6 Conceptual bias in burning rate.

test duration will not be the true average burning rate over the time interval. The burning rate actually changes nonlinearly during the test. An estimate of this effect was made by separating variables and integrating the burning rate equation to determine an analytic expression for web thickness as a function of time. This leads to an analytical expression of the burning rate as a function of time. This burning rate equation was integrated exactly over different test times to determine an exact average burning rate. The exact average burning rate was then compared with the finite difference [Eq. (2)] burning rate.

Figure 6 shows the resulting conceptual bias as a function of test time. For a 2-s burn duration, the bias is 0.16% (exact is lower than finite difference). Quadrupling the test time to 8 s results in a 2% bias. The labscale results based on the finite difference method will overpredict the true average burning rate in the motor. Uncertainties have not been included in this analysis. These results depend upon both the motor port diameter and the assumed burning rate equation of the fuel.

Therefore, when increasing the test time there is a tradeoff. At some point the bias from the conceptual problem of a finite difference burning rate would outweigh the improved test time resolution. This whole discussion, of course, is predicated upon the analysis technique presented. Other methods, such as the use of ultrasonic burning rate measurements or more detailed data analysis are not included in these conclusions.

Another possible conceptual bias is the augmentation of the burning rate from using segmented grains. Some have noted that this can increase the burning rate in Plexiglas® motors. Limited testing[5] with a one-piece, 10-in.-long fuel grain showed no discernible effect on the mass loss for the conditions presented in this article.

Characteristic Velocity and *O/F*

Figure 7 shows a plot of C^* vs *O/F* for several HTPB tests as compared to theoretical C^* values generated using the NASA SP-273 thermochemistry code. The stochiometric *O/F* ratio for HTPB/N-100 is approximately 3.0. Shown in Fig. 7 are the results from tests using 1.0, 4.0, and 0.0 in. or butted aft closure (see Fig. 8) configurations. Data points that lie closer to the theoretical curve would be considered to have higher C^* efficiencies. Thus, on initial inspection of Fig. 6 the conclusion may be drawn that tests conducted using the 4.0-in. closure have higher C^* efficiencies when compared to those using the 1.0-in. or butted aft closure. However, the uncertainty bars on the C^* results indicate that the level of uncertainty does not permit the resolution required to measure a test-to-test difference in C^* for these tests. Thus, no conclusions may be drawn about the effect of instability on the C^* efficiency in the LHM tests. In fact, it is quite possible that efficiencies of greater than 100% could be generated by the LHM according to the uncertainty bars. Finally, the plot shows that for this type of analysis to be worthwhile, uncertainties in the results must be very small (on the order of ±1%), to gain the necessary resolution.

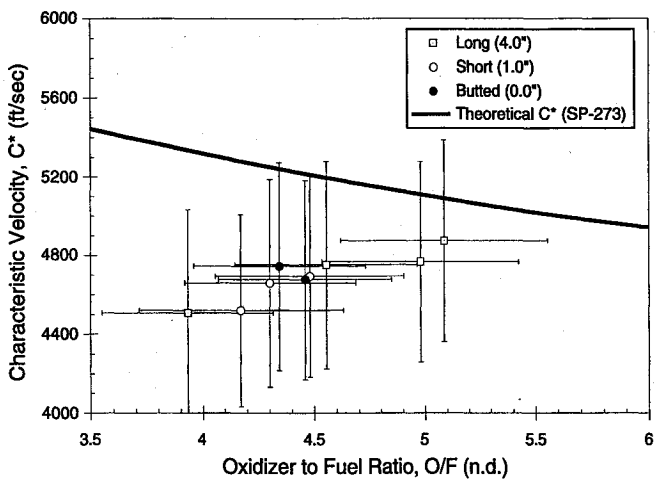

Fig. 7 Plot of C^* vs *O/F* ratio for selected HTPB tests with uncertainty.

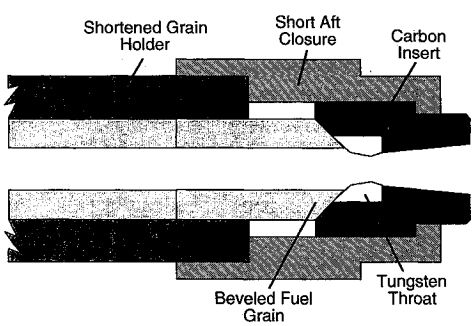

Fig. 8 LHM butted end grain configuration.

Referring again to Tables 3 and 5, by comparing the bias and precision limits for C^* and *O/F*, it is evident that the precision limits contribute to a sizable portion of the overall uncertainties in these two results. This indicates the difficulty of repeating particular test conditions for a comparison of this type. Also, this comparison indicates that reduction of bias contributions in the input parameters is only partially effective. Nevertheless, in examining Table 5 one can see that burning time bias dominates the bias in *O/F* and that C^* bias is dominated by biases in nozzle throat diameter and chamber pressure. Again, increasing the burning duration would reduce the *O/F* bias.

Two methods exist for reducing the C^* bias. The first is to reduce the bias uncertainty in the measurement of the nozzle throat diameter. It is doubtful that the accuracy could be increased because of the small size of the nozzle throat and the fact that the diameter can erode measurably during a test, which would again lead to a conceptual bias. However, increasing the size of the throat, which points to increasing the scale of the motor as a whole, would reduce the sensitivity of the C^* data reduction equation to the throat measurement bias. The second method to reduce the C^* bias is to select a more accurate method for calibrating the chamber pressure data. This will have only a limited effect since the conceptual bias dominates in this reading because of the oscillations that exist even in stable tests, or those with a low level of pressure oscillations. The conceptual bias is even greater for unstable tests in which oscillations of up to ±75 psi (or approximately ±17% of mean P_c) have been noted.[1,4] Another possibility is to test at higher chamber pressures, thus reducing the percent bias in P_c. This would only be effective under the assumption that the absolute bias in chamber pressure remains constant. There is no indication either way as to the validity of this assumption.

Summary of Results and Conclusions

The typical uncertainties in the measurements of the fuel regression rate (±8.7%), oxidizer flux (±10.8%), motor characteristic velocity (±10.5%), and the motor oxidizer-to-fuel mass ratio (±9.2%) are characteristic of the experiments evaluated. Several factors contributed to these uncertainties. First, labscale regression rate/oxidizer flux results are influenced by a high measurement uncertainty in the grain initial port diameter and a large conceptual bias in the burning duration. Second, the low resolution for C^* is because of the measurement uncertainty of the nozzle throat diameter and conceptual bias in the average chamber pressure. Third, the uncertainty of the *O/F* ratio is dominated by the conceptual bias in burn time.

In general, three methods can reduce the uncertainties presented. First, increase the scale of the test motor. This would reduce the uncertainties in the measurements of the diameters of the fuel grain port and nozzle throat. Second, increase the burning duration, which coincidentally could require an increase in the motor size. The increase would reduce the domination of the burning duration conceptual bias. Finally, decrease the uncertainty in the average chamber pressure measurement through either an increase in the test pressure or an improvement in the accuracy of the calibration methodology. However, both of these are believed to have limited effectiveness.

A parametric study of the changes suggested is recommended to determine the magnitude of improvement in the accuracy that could be expected. In addition, this study should indicate the optimal motor configuration for obtaining high-quality hybrid performance data. At minimum, it is clear that all test programs conducting hybrid motor performance mea-

surements must have some level of uncertainty analysis conducted to determine the quality of the data obtained.

Acknowledgments

This work was performed as a follow-up to a program conducted under a Thiokol Corporation IR&D contract to the University of Alabama in Huntsville (UAH) Propulsion Research Center. The authors acknowledge the contributions of Terry Boardman of Thiokol for technical discussions and assistance. The test results came from a cooperative agreement with NASA Marshall Space Flight Center. This analysis was supported by the UAH Propulsion Research Center. The authors recognize the Director of the Center, Clark Hawk, and the Eminent Scholar in Propulsion, Hugh Coleman, whose financial and advisory support made this work possible.

References

[1]Hollman, S., and Frederick, R., "Labscale Testing Techniques for Hybrid Rockets," AIAA Paper 93-2409, June 1993.

[2]Estey, P., Altman, D., and McFarlane, J., "An Evaluation of Scaling Effects for Hybrid Rocket Motors," AIAA Paper 91-2517, June 1991.

[3]Chenevert, D., Taylor, R., and Hodge, B., "Determination of Uncertainties in Thrust-Level Computations of a Hybrid Rocket Motor Model," AIAA Paper 95-2395, June 1995.

[4]Greiner, B. E., and Frederick, R. A., "Experimental Investigation Labscale Hybrid Instability," AIAA Paper 94-2878, June 1994.

[5]Greiner, B. E., "Experimental Investigation of Combustion Instability Using a Labscale Hybrid Rocket Motor," M.S. Thesis, Univ. of Alabama in Huntsville, AL, Oct. 1993.

[6]Coleman, H. W., and Steel, W. G., *Experimentation and Uncertainty Analysis for Engineers*, Wiley, New York, 1989.

[7]Sutton, G., *Rocket Propulsion Elements*, 6th ed., Wiley, New York, 1992, pp. 502–552.